Macromolecules

ARTICLE

pubs.acs.org/Macromolecules

Intramolecular Charge Carrier Mobility in Fluorene-Thiophene Copolymer Films Studied by Microwave Conductivity

Akinori Saeki,*[,†,‡] Takahiro Fukumatsu,[†] and Shu Seki*[,†]

[†]Division of Applied Chemistry, Graduate School of Engineering, Osaka University, 2-1 Yamadaoka, Suita, Osaka 565-0871, Japan

[‡]PRESTO, Japan Science and Technology Agency (JST), 4-1-8 Honcho Kawaguchi, Saitama 332-0012, Japan

Supporting Information

ABSTRACT: The charge carrier mobility along a molecular wire of fluorene-thiophene copolymers represented by poly(9,9′-di-*n*-octylfluorene-*co*-bithiophene): F8T2 is investigated by flash-photolysis time-resolved microwave conductivity. We systematically examined the impacts of the number of oligothiophene units, their composition ratios, and molecular weights. It is revealed that the odd−even number of oligothiophene units has a significant effect on the mobility if they are incorporated into the polyfluorene backbone in high ratio. The structural dependence study and the observed high intramolecular mobility of about 1 $cm^2 V^{-1} s^{-1}$ could be helpful for the design of novel multicomponent conjugated copolymers and its application in organic electronic devices.

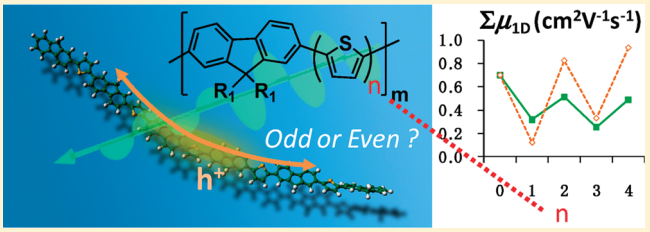

INTRODUCTION

Conjugated polymers have attracted keen attention in recent years due to their potential for low cost, bendable, and large-area via roll-to-roll process organic electronic devices.[1] Multiple-component conjugated polymers consisting of donor−acceptor or push−pull type moieties are highly promising materials as color tunable emitting layers in organic light emitting diodes (OLEDs) and bulk heterojunction frameworks with low-band gap for organic photovoltaic cells (OPVc).[2] Therefore, considerable efforts have been devoted to the development of novel copolymers possessing unique electronic and optical properties. Polyfluorene and its copolymers form an integral part of OLEDs, as they have high absorption coefficient, photoluminescence yield, chemical stability and also due to highly pure blue emission.[3−9] Moreover, their optical properties such as absorption, emission, band gap, the highest occupied molecular orbital (HOMO), and the lowest unoccupied molecular orbital (LUMO) can be easily tuned by the incorporation of appropriate conjugated units into the backbone.

Because of their color tuning property in accordance with the π-conjugation length, fluorene−thiophene (F−T) copolymers have intrigued scientists over a decade. The change of absorption and emission spectra in an F−T amphiphilic block copolymer with the solvent polarity has been demonstrated.[10] The application to OPVc is emerging as one of the most imperative topics for F−T copolymers.[11] The most widely known F−T copolymer is poly(9,9′-dioctylfluorene-*co*-bithiophene), usually abbreviated as F8T2.[12−14] It exhibits a thermotropic and nematic liquid-crystalline behavior above 265 °C, along with relatively high hole mobility (0.02 $cm^2 V^{-1} s^{-1}$). Although optical and electronic property of F8T2 are well-documented, some aspects of those copolymers and also similar other multiple-component π-conjugated semiconducting polymers such as the intrinsic charge transport property along a molecular wire still remain to be addressed.

In the present work, we have investigated intramolecular charge transport of fluorene-thiophene copolymers by electrode-less flash-photolysis time-resolved microwave conductivity (FP-TRMC) technique.[15−17] It measures the nanometer-scale mobility of charge carriers under an oscillating microwave electric field. In the amorphous films state, the maximum mobility before deactivation by trapping along the conjugation length was selectively probed. A systematic investigation on the electronic properties of copolymers were performed, in which the number of thiophene units and its composition ratio were changed in order to elucidate the role of oligothiophene units in the charge transport along the polymer backbone.

RESULTS AND DISCUSSION

The fluorene−thiophene copolymers were synthesized by a Suzuki−Miyaura coupling. Figure 1 shows the chemical structures of the copolymers: pFT*n*−*x*%, where "*n*" represents the number of thiophene units which varies from 0 to 4 and *x*% represents the composition ratio of oligothiophene units. For instance, pFT2−50% is identical to poly(9,9′-dioctylfluorene-*co*-bithiophene), F8T2, although "8" in the latter abbreviation stands for the carbon number of the side alkyl chain (octyl) at the fluorene unit. The case of $n = 0$ (or $x = 0\%$) is poly(9,9′-dioctylfluorene) and

Received: March 3, 2011
Revised: April 1, 2011
Published: April 14, 2011

is represented by pF. The composition ratio of oligothiophene units (x%) was controlled by changing the molar fractions of 2,7-dibromo-9,9-di-*n*-octylfluorene and dibromo oligothiophene during synthesis. The elementary analysis indicates that the composition ratios were almost consistent with the thiophene fractions loaded in a reaction flask (Table 1).

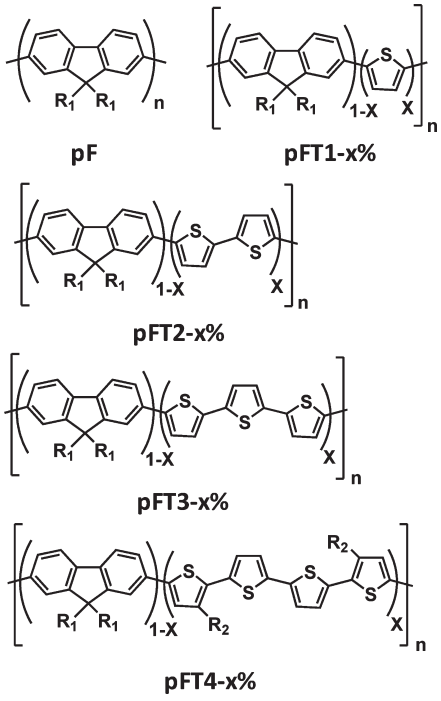

Figure 1. Structures of fluorene−thiophene copolymers: pFTn−x% (n = 0−4, x = 50, 25, 10, and 2%) synthesized by Suzuki−Miyaura coupling. R_1: *n*-octyl. R_2: *n*-hexyl.

Parts a−d of Figure 2 illustrate the steady-state photoabsorption and fluorescence spectra of pFTn−x% (n = 0−4) in chloroform solutions having composition ratio, x = 2, 10, 25, and 50% respectively. The pictures of the corresponding solutions under UV light irradiation are provided in Figure S1, Supporting Information. The band gap energy of the copolymers was estimated from the band edge of the steady-state photoabsorption spectra and the fluorescence peak which are shown in parts e and f of Figure 2, respectively. As shown in Figure 2e, the band gaps of polymers gradually decreased from ca. 2.9 eV of pF to 2.3 eV of pFT4−50%. The fluorescence peaks of pFTn−2% (n = 1−4) shown in Figure 2f were almost identical to that of pF, although a small portion of fluorescence ascribed to the oligothiophene units could be observed at the longer wavelength region. By increasing the ratio of oligothiophene units (>10%) on the polymer backbone, the fluorescence peaks exhibited a distinct red shift with the number of oligothiophene (n). These results imply that excitons can migrate along the polyfluorene over 10 repeating units within their lifetimes, which is in good agreement with the efficient exciton migration along the chain reported in literature.[5]

The transient photoconductivity of the copolymer films was measured by FP-TRMC using a 355 nm nanosecond laser as the excitation source. Figure 3a shows $\phi\Sigma\mu$ transients of pF and pFTn−50% (n = 1−4) films, where ϕ and $\Sigma\mu$ are the quantum efficiency of charge carrier generation and the sum of charge carrier mobilities ($\Sigma\mu = \mu_+ + \mu_-$), respectively. The primary charged species is presumed to be holes ($\Sigma\mu \approx \mu_+ \gg \mu_-$), since the field-effect transistor (FET) or time-of-flight (TOF) studies

Table 1. Optical, Electronic, and Polymeric Properties of Fluorene−Thiophene Copolymers

synonym	M_w (10^4 g mol^{-1})[a]	PDI[b]	monomer unit[c]	thiophene by EA (%)[d]	$\phi\Sigma\mu_{max}$ (10^{-4} cm^2 V^{-1} s^{-1})[e]	ϕ_{max} (10^{-4})[f]	$\Sigma\mu_{1D}$ (cm^2 V^{-1} s^{-1})[g]	λ_{abs} (nm)[h]	λ_{em} (nm)[i]
pF	5.7	2.4	146	-	0.54	2.3	0.70	385	417
pFT1−2%	4.1	2.1	107	0.9	0.30	1.1	0.81	387	418
pFT1−10%	6.6	2.0	182	16.6	0.31	1.4	0.66	391	478
pFT1−25%	3.6	1.8	116	28.4	0.28	2.6	0.32	397	467
pFT1−50%	0.5	1.2	21	52.7	0.09	2.2	0.12	420	469
pFT2−2%	4.0	2.2	104	2.3	0.24	1.1	0.65	387	418
pFT2−10%	5.3	2.2	144	11.7	0.19	0.9	0.63	382	511
pFT2−25%	4.5	2.1	133	27.2	0.26	1.5	0.51	393	493
pFT2−50%	4.2	2.1	153	52.7	0.95	3.4	0.83	454	499
pFT3−2%	4.4	2.1	113	1.8	0.26	1.3	0.58	387	418
pFT3−10%	7.6	2.3	202	10.0	0.23	0.9	0.72	387	539
pFT3−25%	6.5	2.7	184	19.5	0.12	1.5	0.25	387	511
pFT3−50%	0.7	1.6	22	50.6	0.23	2.0	0.33	446	513
pFT4−2%	4.3	2.2	111	2.5	0.25	0.9	0.79	387	418
pFT4−10%	4.8	1.9	120	10.3	0.18	0.9	0.59	388	536
pFT4−25%	7.2	2.2	172	26.1	0.24	1.5	0.49	391	527
pFT4−50%	6.6	2.1	148	49.0	0.67	2.1	0.94	460	533

[a] The weight-averaged molecular weight (M_w) measured by gel permeation chromatography (GPC) using tetrahydrofuran as eluent vs polystyrene standards. [b] Polydispersity index (PDI) measured by GPC. [c] The number of monomer unit calculated by dividing M_w by a molecular weight-averaged over fluorene and oligothiophene considering each composition ratio. [d] The composition ratio of thiophene unit based on the data of elementary analysis (EA). [e] The maximum photoconductivity transients ($\phi\Sigma\mu$) measured by FP-TRMC using 355 nm excitation (9.1×10^{15} cm^{-2} pulse^{-1}). [f] The charge carrier generation efficiency at end-of-pulse (ϕ_{max}) estimated by DC technique with the calibration based on the reported intramolecular mobility of pF. [g] 1-dimensional charge carrier mobility ($\Sigma\mu_{1D}$) calculated from dividing $\phi\Sigma\mu_{max}$ by ϕ_{max} and multiplied by a factor of 3. [h] The steady-state photoabsorption maximum in $CHCl_3$. [i] Fluorescence maximum in $CHCl_3$. The excitation wavelength was 350 nm.

dx.doi.org/10.1021/ma2004844 |*Macromolecules* 2011, 44, 3416–3424

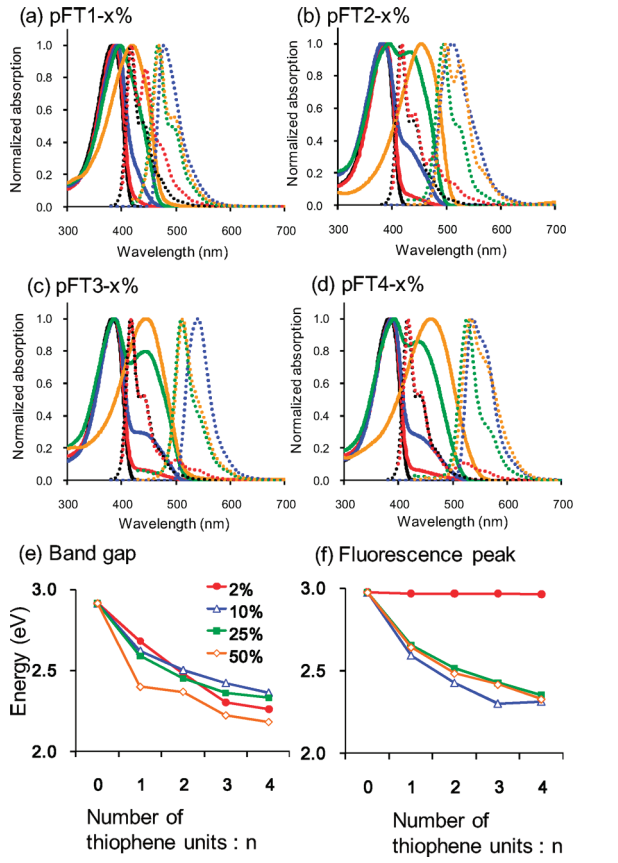

Figure 2. Steady-state photoabsorption (solid line) and fluorescence (dotted line) spectra (λ_{ex} = 350 nm) of (a) pFT1−x%, (b) pFT2−x%, (c) pFT3−x%, and (d) pFT4−x% in chloroform having composition ratio, x = 0% (black), x = 2% (red), x = 10% (blue), x = 25% (green), and x = 50% (orange). The band gap energy of the copolymers estimated from (e) the band edge of the steady-state photoabsorption spectra and (f) the fluorescence peak.

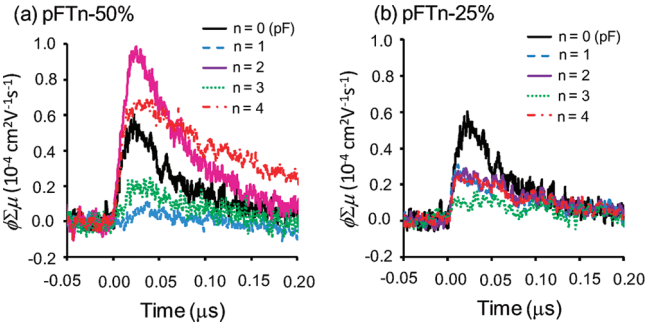

Figure 3. Photoconductivity transients of (a) pFTn−50% and (b) pFTn−25% films measured by FP-TRMC using 355 nm excitation (photon density = 9.1 × 10^{15} cm^{-2} pulse^{-1}). The solid black, blue dashed, purple solid, green dotted, and red dashed lines are n = 0−4, respectively.

of pF and pFT2−50% (F8T2) exhibited p-type characteristics[4,6,12,13] and $\phi\Sigma\mu$ transients were not influenced by air, argon, and SF_6 gases. Except for pFT4−50%, all of the transients exponentially decayed after the end of pulse with a lifetime of ca. 60 ns. This exponential decay was also observed in pFTn−25% (Figure 3b) and other copolymers. Only pFT4−50% exhibited a slow decay which is fitted by second order dynamics rather than first order. Nevertheless, the decay rates of these kinetics were not accelerated by the increase of laser excitation power, as is the case of organic single crystals where the charge carriers decay through bimolecular recombination under their diffusive motions.[16] We therefore concluded that photogenerated charge carriers in fluorene-thiophene copolymers undergoes quick deactivation by trapping sites such as kinks and intermolecular/intersegment energy barriers.

The highest values of $\phi\Sigma\mu$ (i.e., $\phi\Sigma\mu_{max}$) in Figure 3 are therefore considered to reflect the intrinsic charge carrier mobility in the polymers with minimum trapping effects. Polyfluorene has been reported to exhibit a 1-dimensional intramolecular mobility as high as 0.7 cm^2 V^{-1} s^{-1} by pulse radiolysis-TRMC in an insulated and isolated matrix of benzene solution.[15] In contrast, the long-range mobilities are of in the order of $10^{-3} \sim 10^{-4}$ cm^2 V^{-1} s^{-1} as estimated by TOF,[4] FET,[6] and transient photoabsorption spectroscopy.[8] One plausible explanation is that although the stiff backbones of polyfluorenes has a high intramolecular charge mobility on the planner π-orbitals along a relatively long Kuhn segments (segment length = 17.1 nm),[3] on a long-range the charge carriers immediately encounter barriers at the breaking point of π-conjugation and/or at the intermolecular hopping barriers. This can be also corroborated by considering the steric effect of alkyl chains at the 9-position of fluorene, which is perpendicular to the π-plane disturbs the close intermolecular packing. Besides, the neighboring fluorene units are rotated with a torsional angle of 41.6° as calculated by density functional theory (DFT).[7] Nevertheless, the high potential of 1-dimensional intramolecular mobility of polyfluorene motivated us to investigate the effect of incorporated thiophene units on the intramolecular charge transport properties of polyfluorene.

To determine $\Sigma\mu$ of each copolymer, we utilized a direct-current (DC) method in which an interdigitated comb-type gold electrode with 5 μm gaps were used to measure directly the photocurrent generated by 355 nm excitation in spun-cast films under an applied bias of 2 × 10^4 V cm^{-1}.[18] ϕ of pF was calculated on the basis of known 1-dimensional mobility ($\Sigma\mu_{1D}$)[15] as assessed by TRMC in a benzene solution. The ϕ of other copolymers were calibrated by the obtained ϕ of pF (2.3 × 10^{-4}, Figure S2, Supporting Information, and Table 1).

Figure 4a shows $\Sigma\mu_{1D}$ of copolymers plotted against the number of thiophene units. The value of $\phi\Sigma\mu_{max}$ and ϕ_{max} used to calculate $\Sigma\mu_{1D}$ are presented in Table 1 and Figure S3, Supporting Information. The plot of pFTn−50% indicates an "odd-even effect" in which $\Sigma\mu_{1D}$ of the polymers containing odd-numbers thiophene unit (n = 1 and 3) were significantly smaller than the polymers with even numbers of thiophene (n = 0, 2, and 4); however, it should be noted that the effect of the small molecular weight might be convoluted in this result, since the weight-averaged molecular weights (M_w) of pFT1−50% and pFT3−50% are nearly 1 order smaller than the others. These copolymers with high M_w were not successfully synthesized, presumably due to the low reactivity of diboromo thiophene, low solubility of terthiophene, and as well as the conformational disadvantage of the odd-number oligothiophene units (*vide infra*). We examined the impact of M_w on $\Sigma\mu_{1D}$ by preparing pF and pFT2−50% with low and high molecular weights. The $\phi\Sigma\mu_{max}$ increased with M_w as shown in Figure S4a, Supporting Information, mainly due to the increase of ϕ_{max} (Figure S4b, Supporting Information). The obtained $\Sigma\mu_{1D}$ of both pF and

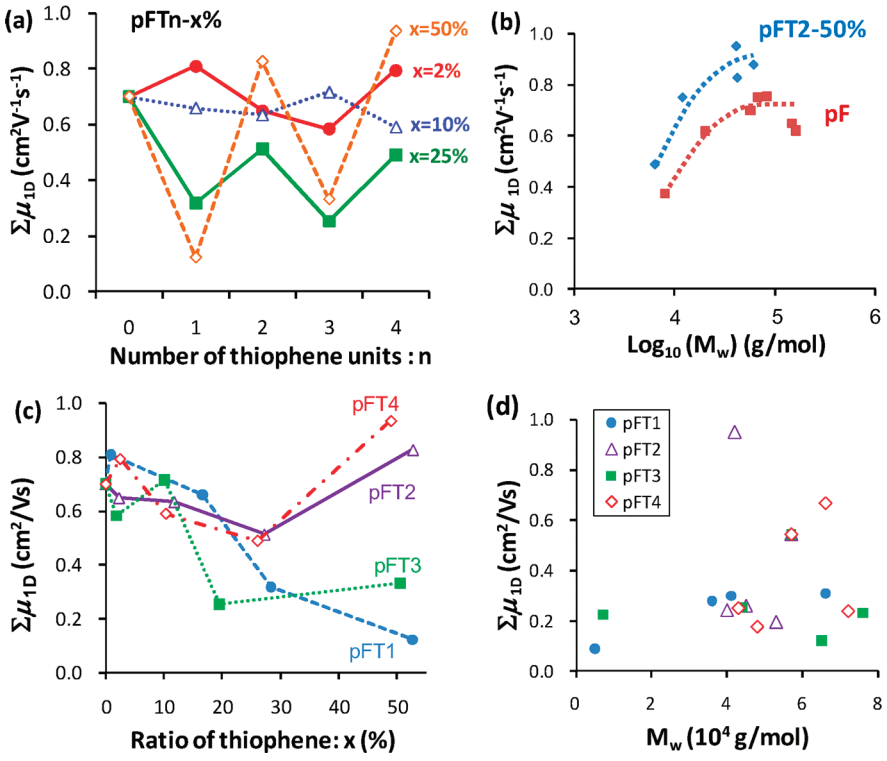

Figure 4. 1-dimensional charge carrier mobility ($\Sigma\mu_{1D}$) of pFTn−x% films estimated from the combination of FP-TRMC and DC techniques. (a) $\Sigma\mu_{1D}$ vs the number of thiophene unit. (b) $\Sigma\mu_{1D}$ vs logarithmic plot of weight-averaged molecular weight (M_w). (c) $\Sigma\mu_{1D}$ are plotted as a function of the composition ratio of thiophene (x%). The values obtained by elementary analysis were used as x%. (d) $\Sigma\mu_{1D}$ are plotted vs M_w without distinguishing the values of x%.

pFT2−50% clearly exhibits an increase followed by a saturation at high M_w (Figure 4b). $\Sigma\mu_{1D}$ values of these polymers were roughly half of each saturated values at M_w = ca. 5×10^3 g mol^{-1} which is close to those of pFT1−50% and pFT3−50%. Therefore, the mobilities of the even-numbered copolymer were still higher than odd numbers, when one compares $\Sigma\mu_{1D}$ at a low M_w.

In order to further confirm the odd−even effect, $\Sigma\mu_{1D}$ of polymers with lower composition ratio of oligothiophene were measured in the same manner. $\Sigma\mu_{1D}$ of pFTn−25% (n = 0−4) was also found to be affected by the odd−even numbers of thiophene units. On the other hand, this effect was almost disappeared for pFTn−10% and pFTn−2%, where their $\Sigma\mu_{1D}$ resembled the values of pF. From the plot of $\Sigma\mu_{1D}$ as a function of the composition ratio, it is clear that the odd−even effect becomes predominant for x > ca. 20% (Figure 4c). The $\Sigma\mu_{1D}$ plot of all copolymers plotted against their M_w is a quite intuitive representation of our claim, wherein $\Sigma\mu_{1D}$ increased roughly with M_w, but they are scattered. (Figure 4d; the similar figures for $\phi\Sigma\mu_{max}$ and ϕ_{max} are provided in Figure S5, Supporting Information).

As described above, $\Sigma\mu_{1D}$ values were estimated from FP-TRMC and DC measurements of pristine films on the basis of the reported $\Sigma\mu_{1D}$ of pF in benzene solution. However, one might cast doubt on the validity of this method by assuming some contribution from intermolecular charge carrier mobility along with the intramolecular process. Hence to rule out this possibility, we prepared pFT4−50% and polystyrene (PS) mixed films by changing the blend ratio from 0.013 to 100 wt % of pFT4−50% relative to 100 wt % PS. We have confirmed that the PS was unable to give a distinct FP-TRMC and transient absorption spectroscopy (TAS) signals on the excitation at 355 nm and also possess a good compatibility with conjugated polymers. Figure 5a shows $\phi\Sigma\mu$ decays observed in the blend films. The difference in the absorbance of each film was compensated according to the reported procedure.[19] Increase of pFT4−50% concentration in PS matrix led to the slight acceleration of the decay rate, probably due to the increase in the density of charge trapping sites. It is of importance that we observed an almost constant $\phi\Sigma\mu_{max}$ over the wide range of blend ratio as shown in Figure 5b. The averaged $\phi\Sigma\mu_{max}$ was ca. 0.52×10^{-4} cm^2 V^{-1} s^{-1},which was close to the value obtained for the pristine pFT4−50% film (0.67×10^{-4} cm^2 V^{-1} s^{-1}). This proves that FP-TRMC mainly probes the intramolecular charge carrier mobility even in the pristine films.

PS acts an insulating matrix, which cannot be used for DC measurements to estimate the charge carrier generation efficiency of the blend films. Therefore, we performed TAS analysis on the blend film on excitation at 355 nm and found a clear transient absorption spectrum centered at ca. 750 nm as shown in Figure 5c. The spectrum shape was not varied by the blend ratio. Figure 5d displays a transient absorption spectrum observed in N_2-saturated toluene solution of pFT4−50%. The absorption maximum is located at ca. 760 nm and the decay follows a first order kinetics with a lifetime of 4.6 μs. The absorption was quenched by O_2-bubbling, confirming that the transient was due to a triplet excited state. The decay profiles observed at 750 nm in the pFT4−50%:PS blend films are shown in Figure 5e, where the vertical axis represents the product of quantum yield (ϕ') and extinction coefficient (ε') of an *intermediate species*, derived from the observed transient photoabsorption, film thickness, steady-state photoabsorption at the excitation wavelength, and TAS

dx.doi.org/10.1021/ma2004844 |*Macromolecules* 2011, 44, 3416–3424

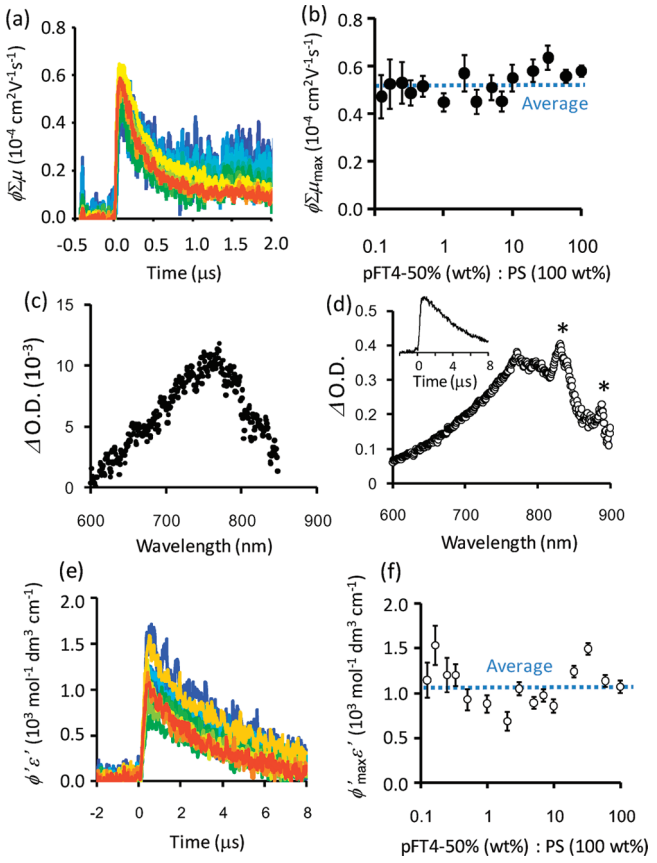

Figure 5. FP-TRMC and TAS studies of the blend films of pFT4−50% and polystyrene (PS) under the excitation at 355 nm. (a) TRMC transients of the blend films (pFT4−50%:PS = 0.013 (blue) − 100 (red): 100 w/w). The difference in the absorbance of each film was compensated according to the reported procedure.[19] (b) Peak of TRMC transients ($\phi\Sigma\mu_{max}$) vs pFT4−50% concentration. The dotted line represents the averaged $\phi\Sigma\mu_{max}$. (c) Transient absorption spectrum (optical density: O.D.) of pFT4−50%:PS = 100:100 film. No significant changes were observed in other blend films. (d) Transient absorption spectrum observed in N_2-bubbled toluene solution of pFT4−50% (1.5 mg mL^{-1}). The peaks labeled by asterisk were artificial, arisen from the characteristic bright line of a Xe lamp. The inset shows the kinetic profile at 760 nm. (e) TAS kinetics of the blend films (pFT4−50%:PS = 0.013 (blue) − 100 (red):100 w/w) monitored at 750 nm. See text for the explanation on ϕ' and ε'. (f) Plot of ($\phi'_{max}\varepsilon'$) vs pFT4−50% concentration. The dotted line represents the averaged $\phi'_{max}\varepsilon'$.

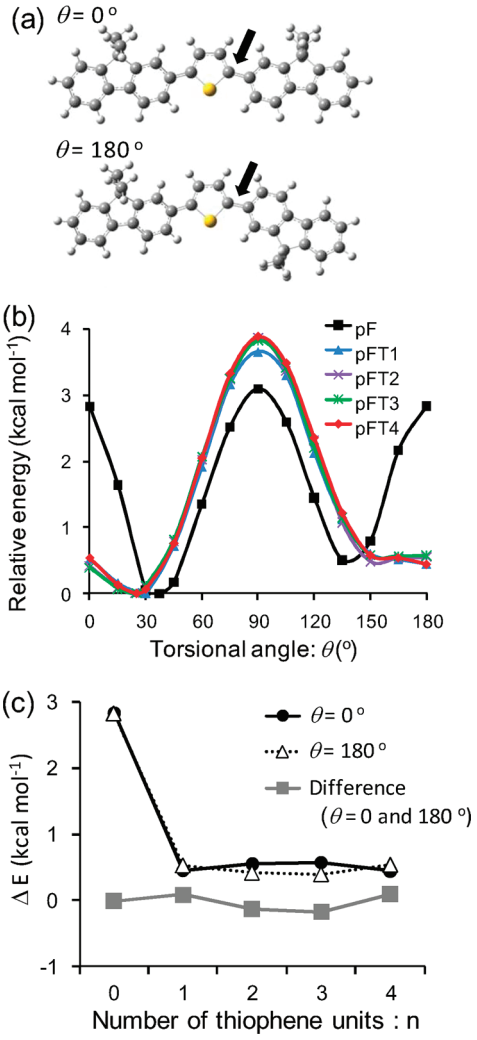

Figure 6. (a) Snapshots of pFT1 trimer with torsional angle θ of 0 and 180 °. The molecular geometry was optimized by DFT using B3LYP/6-31G(d, p) level. The fluorene unit was rotated along the arrowed bond. (b) Torsional potential energy profiles of neutral states of pFT*n* trimers (n = 0−4). The alkyl chains were replaced by methyl substituent for simplicity. (c) The relative energy (ΔE) at θ = 0 ° (black filled circle and black solid line) and 180 ° (open triangle and black dotted line). The gray square and line indicate the energy difference between θ = 0 and 180°.

geometry, according to the reported procedure.[19] All of the profiles were fitted by a first order decay, giving lifetime values in the range of 2.8 - 4.4 μs (the average was 3.8 μs) which is much longer than the decay of FP-TRMC transients (Figure 5a). Although both radical cation and anion have the absorption maxima at ca. 790 nm (Figure S6, Supporting Information), the absorption found in the pFT4−50%:PS blend films was ascribable mainly to the triplet state by considering the lifetime and the spectrum peak. The maximum $\phi'\varepsilon'$ (= $\phi'_{max}\varepsilon'$) was extracted and plotted as a function of pFT4−50% concentration in Figure 5f. No distinct trend could be observed, indicating that the triplet quantum yield is not changed significantly by the blend ratio, suggesting that the charge carrier generation efficiency (ϕ) does not vary considerably with the latter.

Since the thiophene ring has a bended bond direction at its 2 and 5 positions, its incorporation in odd and even numbers in a polymer backbone could lead to different molecular packing in crystalline phase. There are several reports based on the dependence of odd−even effects on thermal, optical, and electrical properties of conjugated materials. For example, it has been reported that the crystal densities of the even-numbered oligothiophenes are slightly higher than those of odd-number.[20] The systematic investigation on the effect of odd−even numbers of thiophene units on the bulk crystalline properties were reported by Clot et al. in oligothiophenes (n = 1−6) capped with two dibutylaminostyryl moieties, where they observed an increase in the melting points of even-numbered oligomers (about 50 °C) when compared to that of odd-numbered ones.[21] Regarding the electronic properties, Nagamatsu et al.[22] have performed FET studies on unsubstituted oligothiophenes (n = 5−7), showing that the FET mobilities of even-numbered oligothiophenes were improved, due to the proper structural

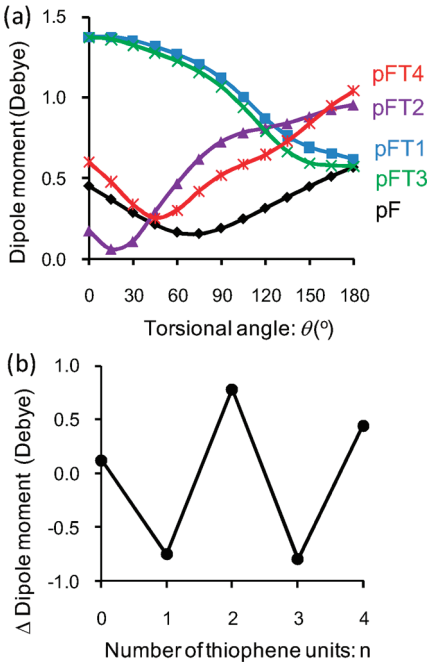

Figure 7. (a) Dipole moments of neutral states of pFT*n* trimers (*n* = 0−4) vs torsional angle calculated with DFT using B3LYP/6-31G(d, p) level. (b) Difference of dipole moments between 180 and 0°.

Scheme 1. Polymerization of Fluorene/Thiophene Copolymers: pFT*n*−*x*%[a]

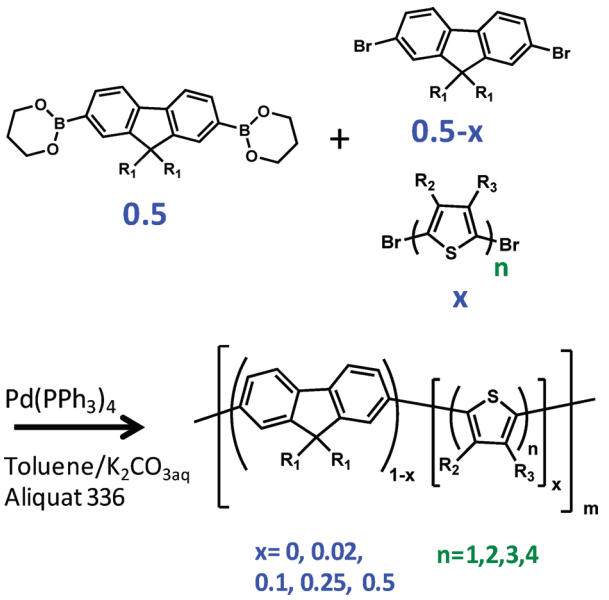

[a] R_1: *n*-octyl. R_2: H for pFT1, pFT2, and pFT3. In the case of pFT4, R_2 = H and R_3 = *n*-hexyl for *n* = 1; R_2, R_3 = H for *n* = 2 ∼ 3; and R_2 = *n*-hexyl, R_3 = proton for *n* = 4.

ordered arrangement. Bao's group[23] has demonstrated better FET mobilties of the even-numbered 5,5′-bis(7-hexyl-9*H*-fluoren-2-yl)-2,2′-oligothiophenes (*n* = 1−4). He et al.[24] have synthesized the fused thiophene (*n* = 3−5) and bithiophene copolymers and showed that the FET mobilities of even-numbered derivatives were superior to those of odd-numbered derivatives. All of these reports dealt with the advantage of even-numbered thiophenes in the intermolecular charge transport, which arises due to the favorable packing of their crystalline structures. In contrast, we herein focus on the intramolecular charge mobility which would be affected mainly by the feature of a single polymer chain rather than its packing structure.

The chain conformations of F−T copolymers were established with density functional theory (DFT) using B3LYP/6-31G(d, p) level. The torsional potential energy profiles of neutral states of fluorene−thiophene−fluorene trimers were calculated. One of the fluorene units was rotated after the geometry optimization (Figure 6a). As shown in Figure 6b, The neutral pF trimer has a minimum energy at the torsion angle (θ) of 37°, due to the repulsive force of protons of neighboring aromatic rings, while the other trimers take more planar structures with the minimum θ of 24−30°. This planarity of pFT*n* (*n* = 1−4) trimers is more pronounced for their cationic states (Figure S7). These results rationalize the slightly higher $\Sigma\mu_{1D}$ of pFT2−50% and pFT4−50% than that of pF (Figure 4a). The $\Sigma\mu_{1D}$ decreased by increasing the composition ratio of fluorene units which insert a twisted site into the copolymer backbone. The DFT calculations of the neutral states were, however, not indicative of the odd−even effect in the minimum θ, the relative energies at θ = 0 and 180° (Figure 5c), and the potential barriers of the rotation at θ = 90° (3−4 kcal mol^{-1}).

Since both thiophene and fluorene units have a tilted angle of bond direction, the direction of dialkyl chains at the fluorene unit might be affected by the number of oligothiophene units. As shown in Figure 6a, the alkyl chains were placed at one side for the odd-numbered copolymers (e.g., pFT1), while they occupy at opposite sides in the even-numbered copolymers (e.g., pFT2) when the conjugated units were aligned in a straight manner (θ = 0°). The energy difference between θ = 0 and 180° was estimated as small as ca. 0.4 kcal mol^{-1} by the DFT, suggesting that both conformations are stable. However, the linearity of polymer backbone is largely affected by the parity of oligothiophene units. This is visualized by the relative change of dipole moments of trimers, whereas the odd-numbered trimers showed a decrease of dipole by the rotation from θ = 0 to 180° in contrast to an increase for the even-numbered trimers (Figures 7). The alkyl side chains of conjugated polymers have been known for not only to improve their solubility but also to change the backbone conformations, leading to solvatochromism, thermochromism, etc.[25] The rotation of the fluorene units in a an odd-numbered pFT*n* to make the alkyl chains in opposite directions to maximize the interaction with solvents distorts the polymer backbone as shown in the lower part of Figure 6a and hence reduces the charge carrier motion parallel to the direction of electric field of probing microwave. The drawback of shrunk conformation of main chain was also confirmed from the FP-TRMC experiment, in which photoconductivity of pFT2−50% powder precipitated in methanol was decreased to ca. 30% of the film (Figure S8, Supporting Information).

The performance of organic electronic devices depends considerably on the intermolecular charge carrier transport enhanced by strong and well-defined packing. However, we believe that a molecular design giving high intramolecular charge mobility is also important to maximize the capability of organic electronics frameworks for their further improvements.

dx.doi.org/10.1021/ma2004844 |*Macromolecules* 2011, 44, 3416–3424

CONCLUSION

The intramolecular mobilities of charge carrier in fluorene−thiophene copolymer films were investigated by FP-TRMC technique. The important observation was that the charge carrier mobilities of copolymers with the even-numbered oligothiophene units with composition ratios of 50 and 25% are higher than those of the odd-number polymers. This is correlated with the tilted bond direction of thiophene and fluorene rings and the resultant alternating symmetry of the alkyl chains at the fluorene unit. Interestingly, this odd−even effect disappeared and the mobility converged to ca. 0.7 $cm^2\ V^{-1}\ s^{-1}$ once the oligothiophene composition ratio was decreased to less than 10%. It should be emphasized that the mobility decreases in the polymers with M_w less than 10^4 g mol^{-1}. We do hope these findings are extremely important from the point of view of designing copolymers for various applications like OPVc and OLEDs.

EXPERIMENTAL SECTION

General Procedure of Polymerization. Unless otherwise noted, reagents and solvents were used as received from Aldrich and Wako Chemical, respectively. Scheme 1 shows the general procedure of polycondensation. 9,9-di-*n*-octylfluorene-2,7-diboronic acid bis(1,3-propanediol) ester [0.2 mmol], 2,7-dibromo 9,9-dioctylfluorene [0.2 × (0.5−*x*) mmol], 2,5-dibromo thiophene oligomer [0.2 × *x* mmol], $Pd(PPh_3)_4$ [0.02 mmol, Tokyo Chemical Industry Corp.], 5 mL of 2 M K_2CO_3 aqueous solution, Aliquat336 [0.12 mmol] and toluene, 10 mL, were placed in a 50 mL flask. Note that *x* represents the ratio of thiophene unit, for example *x* is 0.02 for pFT*n*−2%. The reaction solution was vigorously degassed by the freeze−pump−thaw method before polymerization was started. The mixture was heated at 85 °C for 12−24 h. In the case to obtain low-molecular weight polymers, the polymerization was stopped at an appropriate time. The reaction mixture was poured into methanol. The precipitate was collected and then extracted by toluene with ammonia solution, 1 N HCl_{aq}, and water. The combined organic extract was dried over anhydrous $MgSO_4$, and filtered off from an insoluble fraction. The polymer solution was subjected to Celite chromatography and stirred for 24 h with Pd scavenger. The polymer was precipitated again in methanol.

5,5‴-Dibromo-3,3‴-dihexyl-2,2′:5′,2″:5″,2‴-quaterthiophene. Except for quarterthiophene, dibromo-oligothiophenes are commercially available and were used as received. To a *N*,*N*′-dimethylformamide solution (10 mL) of 3,3‴-dihexyl-2,2′:5′,2″:5″,2‴-quaterthiophene (2 mmol) was portionwise added *N*-bromosuccinimide (NBS, 4.5 mmol) at −20 °C under argon, and the mixture was allowed to warm to 60 °C. After 20 h of stirring, the reaction mixture was poured into an aqueous solution of KOH (10%, 100 mL) and extracted with toluene. The combined organic extract was washed with water, dried over anhydrous $MgSO_4$, and filtered off from an insoluble fraction. The filtrate was evaporated to dryness under a reduced pressure, and the residue was subjected to column chromatography (SiO_2, AcOEt/hexane 7/3 v/v), to allow isolation of dibromo-quarterthiophene as yellow-orange powder in 80% yield. ^{1}H NMR (270 MHz, $CDCl_3$): δ (ppm) 7.10 (d, J = 2 Hz, 2H), 7.00 (d, J = 2 Hz, 2H), 6.90 (s, 2H), 2.71 (t, J = 8 Hz, 4H), 1.61 (t, J = 8 Hz, 4H), 1.32 (m, 12H), 0.89 (t, J = 7 Hz, 6H). FAB-mass: calcd for $C_{28}H_{32}Br_2S_4$, 656.62; found, 656.04.

F8 Polymer: Poly(9,9′-di-*n*-octylfluorenyl-2,7-diyl). White powders were obtained in 20−50% yield depending on molecular weight. ^{1}H NMR (270 MHz, $CDCl_3$): δ (ppm) 7.97−7.77 (br), 7.76−7.63 (br), 2.30−1.85 (br), 1.59−1.47 (br), 1.33−0.98 (br). Anal. Calcd for $(C_{29}H_{40})_n$: C, 89.63; H, 10.37. Found: C, 88.83; H, 11.17. Weight-averaged molecular weights (M_w) and polydispersity index (PDI) were 2.0 × 10^4 (2.0), 5.7 × 10^4 (2.4), 6.7 × 10^4 (3.1), 8.3 × 10^4 (3.7), 15 × 10^4 (3.8), and 16 × 10^4 (3.6) g/mol.

pFT1−*x*% Polymer: Poly(9,9′-di-*n*-octylfluorene-*co*-thiophene). Yellow-green clay (pFT1−2%, yield 48%), yellow-green powder (pFT1−10%, yield 51%), yellow-green powder (pFT1−25%, yield 43%), and red clay (pFT1−50%, yield 22%) were obtained. ^{1}H NMR (270 MHz, $CDCl_3$): δ (ppm) pFT1−2%, 7.99−7.47 (br), 2.37−1.80 (br), 1.59−1.47 (br), 1.33−0.99 (br), 0.99−0.69 (br); pFT1−10%, 7.96−7.47 (br), 2.26−1.94 (br), 1.59−1.47 (br), 1.30−1.05 (br), 0.92−0.73 (br); pFT1−25%, 7.95−7.32 (br), 2.29−1.94 (br), 1.59−1.47 (br), 1.36−1.00 (br), 0.97−0.60 (br); pFT1−50%, 7.93−7.34 (br), 2.21−1.92 (br), 1.59−1.47 (br), 1.30−0.87 (br), 0.87−0.62 (br). Anal. Calcd for pFT1−2%: C, 89.49; H, 10.34; S, 0.16. Found: C, 89.69; H, 10.24; S, 0.07. Anal. Calcd for pFT1−10%: C, 88.98; H, 10.21; S, 0.81. Found: C, 88.38; H, 10.04; S, 1.58. Anal. Calcd for pFT1−25%: C, 88.06; H, 9.98; S, 1.96. Found: C, 87.33; H, 9.66; S, 3.00. Anal. Calcd for pFT1−50%: C, 84.20; H, 8.99; S, 6.81. Found: C, 82.01; H, 10.15; S, 7.84. The molecular ratios of thiophene unit calculated from the elementary analysis were 0.9% for pFT1−2%, 16.6% for pFT1−10%, 28.4% for pFT1−25%, and 52.7% for pFT1−50%. M_w (PDI) of pFT1−2%, pFT1−10%, pFT1−25%, and pFT1−50% were 4.1 × 10^4 (2.1), 6.6 × 10^4 (2.0), 3.6 × 10^4 (1.8), and 5.0 × 10^3 (1.2) g/mol, respectively.

pFT2−*x*% Polymer: Poly(9,9′-di-*n*-octylfluorene-*co*-bithiophene). Green clay (pFT2−2%, yield 33%), yellow-green powder (pFT2−10%, yield 25%), bright yellow powder (pFT2−25%, yield 48%), and orange powder (pFT2−50%, yield 30−50%, depending on the molecular weight) were obtained. ^{1}H NMR (270 MHz, $CDCl_3$): δ (ppm) pFT2−2%, 7.96−7.41 (br), 2.32−1.87 (br), 1.59−1.47 (br), 1.33−0.98 (br), 0.93−0.68 (br); pFT2−10%, 7.89−7.41 (br), 2.22−1.96 (br), 1.59−1.47 (br), 1.22−1.02 (br), 0.92−0.70 (br); pFT2−25%, 7.93−7.30 (br), 2.29−1.89 (br), 1.59−1.47 (br), 1.26−0.97 (br), 0.97−0.72 (br); pFT2−50%, 7.84−7.01 (br), 2.22−1.88 (br), 1.59−1.47 (br), 1.29−0.94 (br), 0.88−0.65 (br). Anal. Calcd for pFT2−2%: C, 89.36; H, 10.31; S, 0.33. Found: C, 89.49; H, 10.13; S, 0.38. Anal. Calcd for pFT2−10%: C, 88.36; H, 10.05; S, 1.58. Found: C, 88.10; H, 9.84; S, 2.07. Anal. Calcd for pFT2−25%: C, 86.65; H, 9.62; S, 3.73. Found: C, 85.30; H, 9.36; S, 5.34. Anal. Calcd for pFT2−50%: C, 80.38; H, 8.02; S, 11.60. Found: C, 79.41; H, 8.00; S, 12.59. The molecular ratios of thiophene unit calculated from the elementary analysis were 2.3% for pFT2−2%, 11.7% for pFT2−10%, 27.2% for pFT2−25%, and 52.7% for pFT2−50%. M_w (PDI) of pFT2−2%, pFT2−10%, and pFT2−25% were 4.0 × 10^4 (2.2), 5.3 × 10^4 (2.2), and 4.5 × 10^4 (2.1) g/mol, respectively. M_w (PDI) of pFT2−50% were varied from 6.4 × 10^3 (1.7), 1.2 × 10^4 (1.6), and 4.1 × 10^4 (2.1), to 4.2 × 10^4 (2.1).

pFT3−*x*% Polymer: Poly(9,9′-di-*n*-octylfluorene-*co*-terthiophene). Yellow-green clay (pFT3−2%, yield 43%), ocher clay (pFT3−10%, yield 36%), bright orange powder (pFT3−25%, yield 47%), and dark red clay (pFT3−50%, yield 15%) were obtained. ^{1}H NMR (270 MHz, $CDCl_3$): δ (ppm) pFT3−2%, 8.02−7.29 (br), 2.36−1.87 (br), 1.59−1.47 (br), 1.32−1.00 (br), 0.94−0.72 (br). pFT3−10%: 8.00−7.12 (br), 2.45−1.83 (br), 1.30−1.00 (br), 0.92−0.70 (br); pFT3−25%, 7.95−7.01 (br), 2.33−1.85 (br), 1.59−1.47 (br), 1.33−0.95 (br), 0.95−0.57 (br); pFT3−50%, 7.73−7.08 (br), 2.13−1.87 (br), 1.59−1.47 (br), 1.32−0.92 (br), 0.92−0.57 (br). Anal. Calcd for pFT3−2%: C, 89.16; H, 10.38; S, 0.45. Found: C, 89.49; H, 10.13; S, 0.38. Anal. Calcd for pFT3−10%: C, 87.77; H, 9.90; S, 2.33. Found: C, 87.62; H, 9.80; S, 2.58. Anal. Calcd for pFT3−25%: C, 85.37; H, 9.29; S, 5.34. Found: C, 85.49; H, 9.31; S, 5.20. Anal. Calcd for pFT3−50%: C, 77.55; H, 7.30; S, 15.15. Found: C, 77.36; H, 7.25; S, 15.39. The molecular ratios of thiophene unit calculated from the elementary analysis were 1.8% for pFT3−2%, 10.1% for pFT3−10%, 19.5% for pFT3−25%, and 50.6% for pFT3−50%. M_w (PDI) of pFT3−2%,

pFT3−10%, pFT3−25%, and pFT3−50% were 4.4×10^4 (2.1), 7.6×10^4 (2.3), 6.5×10^4 (2.7), and 7.1×10^3 (1.6) g/mol, respectively.

pFT4−*x*% Polymer: Poly[9,9′-di-*n*-octylfluorene-*co*-(3,3‴-dihexyl-2,2′:5′,2″:5″,2‴-quaterthiophene)]. Dark yellow-green clay (pFT4−2%, yield 38%), yellow powder (pFT4−10%, yield 43%), bright orange powder (pFT4−25%, yield 45%), and red powder (pFT4−50%, yield 53%) were obtained. ^{1}H NMR (270 MHz, $CDCl_3$): δ (ppm) pFT4−2%, 8.03−7.31 (br), 7.22−7.06 (br), 2.93−2.79 (br), 2.38−1.86 (br), 1.82−1.69 (br), 1.60−1.48 (br), 1.42−1.33 (br), 1.32−0.99 (br), 0.95−0.89 (br), 0.88−0.67 (br); pFT4−10%, 7.98−7.38 (br), 7.21−7.00 (br), 2.95−2.68 (br), 2.34−1.83 (br), 1.82−1.67 (br), 1.56−1.43 (br), 1.42−1.32 (br), 1.27−0.97 (br), 0.95−0.89 (br), 0.86−0.57 (br); pFT4−25%, 7.94−7.40 (br), 7.20−7.05 (br), 2.97−2.70 (br), 2.28−1.86 (br), 1.83−1.61 (br), 1.49−1.31 (br), 1.26−0.99 (br), 0.95−0.86 (br), 0.85−0.67 (br); pFT4−50%, 7.77−7.38 (br), 7.21−6.94 (br), 2.95−2.63 (br), 2.15−1.86 (br), 1.84−1.55 (br), 1.53−1.39 (br), 1.39−1.27 (br), 1.25−0.95 (br), 0.95−0.84 (br), 0.85−0.57 (br). Anal. Calcd for pFT4−2%: C, 89.08; H, 10.28; S, 0.64. Found: C, 89.11; H, 10.09; S, 0.80. Anal. Calcd for pFT4−10%: C, 87.14; H, 9.93; S, 2.93. Found: C, 86.90; H, 9.80; S, 3.30. Anal. Calcd for pFT4−25%: C, 84.31; H, 9.43; S, 6.25. Found: C, 83.18; H, 8.90; S, 7.92. Anal. Calcd for pFT4−50%: C, 77.32; H, 8.20; S, 14.49. Found: C, 77.30; H, 8.38; S, 14.31. The molecular ratios of thiophene unit calculated from the elementary analysis were 2.5% for pFT4−2%, 10.3% for pFT4−10%, 26.1% for pFT4−25%, and 49.0% for pFT4−50%. M_w (PDI) of pFT4−2%, pFT4−10%, pFT4−25%, and pFT4−50% were 4.3×10^4 (2.2), 4.8×10^4 (1.9), 7.2×10^4 (2.2), and 6.6×10^4 (2.1) g/mol, respectively.

General Measurements. UV−vis absorption and fluorescence spectroscopies were performed using a JASCO model V-570 and a Hitachi model F-2700 spectrometers, respectively. Polymers were dissolved in spectroscopy-grade chloroform purchased from Wako Chemical Corporation and bubbled by argon gas for at least 10 min. Gel permeation chromatography (GPC) of a Hitachi model (L-2455, L-2130, and L-2350) was performed in tetrahydrofuran (THF) solutions. The molecular weights were calculated using a calibration curve based on polystyrene standards purchased from Aldrich. Nuclear magnetic resonance (NMR) spectroscopy was performed by a JEOL model 270 MHz NMR instrument. Fast atom bombardment (FAB) mass spectroscopy was performed by a JEOL model JSM-700.

Film Preparation. Copolymer films were prepared on a quartz plate by drop-cast from 2 wt % chlorobenzene solutions. The films were dried in a vacuum oven at 60 °C. Polystyrene ($M_w = 2.8 \times 10^5$) was purchased from Aldrich. The blend films of pFT4−50% and polystyrene were prepared in the same manner from the mixed chlorobenzene solutions.

Flash-Photolysis Time-Resolved Microwave Conductivity. Transient photoconductivity was measured by flash-photolysis time-resolved microwave conductivity (FP-TRMC).[15−17] A resonant cavity was used to obtain a high degree of sensitivity in the measurement of conductivity. The resonant frequency and the microwave power were set at ∼9.1 GHz and 3 mW, respectively, so that the electric field of the microwave was sufficiently small not to disturb the motion of charge carriers. The value of conductivity is converted to the product of the quantum yield: ϕ and the sum of charge carrier mobilities: $\Sigma\mu$, by $\phi\Sigma\mu = \Delta\sigma\,(eI_0F_{light})^{-1}$, where e, I_0, F_{Light}, and $\Delta\sigma$ are the unit charge of a single electron, incident photon density of excitation laser (photons/m^2), a correction (or filling) factor (/m), a transient photoconductivity, respectively. The change of conductivity is equivalent with $\Delta P_r/(AP_r)$, where ΔP_r, P_r, and A area change of reflected microwave power, a power of reflected microwave, and a sensitivity factor [(S/m)$^{-1}$], respectively. Third harmonic generation (THG, 355 nm) of a Nd:YAG laser (Spectra Physics Inc. INDY, 5−8 ns pulse duration) was used as an excitation source. The incident photon density was changed from 0.91 to 9.1×10^{15} photons/cm^2. The data in the text and this Supporting Information were observed at 9.1×10^{15} photons/cm^2. The sample was set at the highest electric field in a resonant cavity. The experiments were carried out at room temperature.

Flash-Photolysis Transient Absorption Spectroscopy. Transient absorption spectroscopy (TAS) was performed by using third harmonic generation (THG, 355 nm) of a Nd:YAG laser (Spectra Physics Inc. INDY, 5−8 ns pulse duration) as an excitation and a white light continuum from a Xe lamp as a probe light. The probe light was guided into a wide-dynamic-range streak camera (Hamamatsu C7700) which collects two-dimensional image of the spectrum and time profiles of light intensity. In the solution study, the excitation laser and probe light were aligned by cross-sectional geometry. The solution was bubbled by N_2 for 5 min and loaded in a 1×1 cm^2 quartz cell with seal.

Direct Current-Integration. An interdigitated comb-type gold electrode with 5 μm gaps, 40 nm height, and 2 mm width fabricated by lithographic process in the laboratory was used for direct-current (dc) integration experiments.[18] After an appropriate cleaning including UV-ozone treatment, thin polymer film was cast on an electrode by spin-coating of chlorobenzene solution of 1 wt % polymer with 1500 rpm for 10 min. Thickness of film was measured by a stylus surface profiler (ULVAC, Dektak 150), giving ca. 50 nm. We confirmed that gaps of interdigitated electrode were filled by polymer from a surface observation. An electrode was placed in a vacuum prober and exposed to the same laser with FP-TRMC experiment. The applied bias was controlled by an Advantest Corp. model R8252 digital electrometer. The transient photocurrent was measured by a Tektronix digital oscilloscope equipped with termination resistance. The applied bias and incident photon density of 355 nm laser were 2×10^4 V/cm and 9.1×10^{15} photons/cm^2, respectively. The experiments were carried out at room temperature.

Density Functional Theory (DFT). For the molecular orbital simulations, DFT calculations were performed using the Gaussian03 Rev. E.01 package. The B3LYP and UB3LYP functions with 6-31G(d,p) basis set were used for neutral and cationic states of pFT*n* trimers, respectively. The alkyl side chains were replaced by methyl for simplicity.

■ ASSOCIATED CONTENT

Supporting Information. Figures S1−S8, showing steady-state photoabsorption and emission spectra, photocurrent signals, photoconductivity transients, absorption spectra, torsional potential energy profiles, and relative energies. This material is available free of charge via the Internet at http://pubs.acs.org.

■ AUTHOR INFORMATION

Corresponding Author

*E-mail: (A.S.) saeki@chem.eng.osaka-u.ac.jp; (S.S.) seki@chem.eng.osaka-u.ac.jp.

■ ACKNOWLEDGMENT

This work was supported in part by PRESTO-JST and KAKENHI from the MEXT, Japan. The authors would like to thank Dr. Toshihiro Okamoto at Osaka University for advising about the polymer synthesis. We would like to thank Dr. Chakooth Vijayakumar and Dr. Balan Bijitha for helpful discussion.

REFERENCES

(1) (a) Coropceanu, V.; Cornil, J.; da Silva Filho, D. A.; Olivier, Y.; Silbey, R.; Brédas, J.-L. *Chem. Rev.* **2007**, *107*, 926. (b) Argun, A. A.; Aubert, P. -H.; Thompson, B. C.; Schwendeman, I.; Gaupp, C. L.; Hwang, J.; Pinto, N. J.; Tanner, D. B.; MacDiarmid, A. G.; Reynolds, J. R. *Chem. Mater.* **2004**, *16*, 4401. (c) Wheeler, S. E.; McNeil, A. J.; Müller, P.; Swager, T. M.; Houk, K. N. *J. Am. Chem. Soc.* **2010**, *132*, 3304. (d) Tulek, A.; Polson, R. C.; Vardeny, Z. V. *Nature Phys.* **2010**, *6*, 303.

(2) (a) Kim, J. Y.; Lee, K.; Coates, N. E.; Moses, D.; Nguyen, T.-Q.; Dante, M.; Heeger, A. J. *Science* **2007**, *317*, 222. (b) Inganäs, O.; Zhang, F.; Andersson, M. R. *Acc. Chem. Res.* **2009**, *42*, 1731. (c) Dennler, G.; Scharber, M. C.; Brabec, C. J. *Adv. Mater.* **2009**, *21*, 1323. (d) Bijleveld, J. C.; Zoombelt, A. P.; Mathijssen, S. G. J.; Wienk, M. M.; Turbiez, M.; de Leeuw, D. M.; Janssen, R. A. J. *J. Am. Chem. Soc.* **2009**, *131*, 16617. (e) Chen, H. -Y.; Hou, J.; Zhang, S.; Liang, Y.; Yang, G.; Yang, Y.; Yu, L.; Wu, Y.; Li, G. *Nature Photo* **2009**, *3*, 649. (f) Piliego, C.; Holcombe, T. W.; Douglas, J. D.; Woo, C. H.; Beaujuge, P. M.; Fréchet, J. M. J. *J. Am. Chem. Soc.* **2010**, *132*, 7595. (g) Jiang, Y.; Okamoto, T.; Becerril, H. A.; Hong, S.; Tang, M. L.; Mayer, A. C.; Parmer, J. E.; McGehee, M. D.; Bao, Z. *Macromolecules* **2010**, *43*, 6361.

(3) Grell, M.; Bradley, D. D. C.; Long, X.; Chamberlain, T.; Inbasekaran, M.; Woo, E. P.; Soliman, M. *Acta Polym.* **1998**, *49*, 439.

(4) Redecker, M.; Bradley, D. D. C.; Inbasekaran, M.; Woo, E. P. *Appl. Phys. Lett.* **1999**, *74*, 1400.

(5) (a) Lyons, B. P.; Monkman, A. P. *Phys. Rev. B* **2005**, *71*, 235201. (b) Shibano, Y.; Imahori, H.; Sreearunothai, P.; Cook, A. R.; Miller, J. R. *J. Phys. Chem. Lett.* **2010**, *1*, 1492.

(6) Yasuda, T.; Fujita, K.; Tsutsui, T.; Geng, Y.; Culligan, S. W.; Chen, S. H. *Chem. Mater.* **2005**, *17*, 264.

(7) Fratiloiu, S.; Grozema, F. C.; Koizumi, Y.; Seki, S.; Saeki, A.; Tagawa, S.; Dudek, S. P.; Siebbeles, L. D. A. *J. Phys .Chem. B* **2006**, *110*, 5984.

(8) Asaoka, S.; Takeda, N.; Iyoda, T.; Cook, A. R.; Miller, J. R. *J. Am. Chem. Soc.* **2008**, *130*, 11912.

(9) Moynihan, S.; Lovera, P.; O'Carroll, D.; Iacopino, D.; Redmond, G. *Adv. Mater.* **2008**, *20*, 2497. (b) Scherf, U.; Gutacker, A.; Koenen, N. *Acc. Chem. Res.* **2008**, *41*, 1086. (c) Simon, S. C.; Schmaltz, B.; Rouhanipour, A.; Räder, H. J.; Müllen, K. *Adv. Mater.* **2009**, *21*, 83. (d) Tachibana, Y.; Makuta, S.; Otsuka, Y.; Terao, J.; Tsuda, S.; Kambe, N.; Seki, S.; Kuwabata, S. *Chem. Commun.* **2009**, 4360. (e) Zhou, E.; Cong, J.; Yamakawa, S.; Wei, Q.; Nakamura, M.; Tajima, K.; Yang, C.; Hashimoto, K. *Macromolecules* **2010**, *43*, 2873.

(10) Tu, G.; Li, H.; Forster, M.; Heiderhoff, R.; Balk, L. J.; Sigel, R.; Scherf, U. *Small* **2007**, *3*, 1001.

(11) (a) Yao, K.; Chen, Y.; Chen, L.; Zha, D.; Li, F.; Pei, J.; Liu, Z.; Tian, W. *J. Phys. Chem. C* **2010**, *114*, 18001. (b) Bu, L.; Guo, X.; Yu, B.; Qu, Y.; Xie, Z.; Yan, D.; Geng, Y.; Wang, F. *J. Am. Chem. Soc.* **2009**, *131*, 13242. (c) Shi, C.; Yao, Y.; Yang, Y.; Pei, W. *J. Am. Chem. Soc.* **2006**, *128*, 8980.

(12) Sirringhaus, H.; Wilson, R. J.; Friend, R. H.; Inbasekaran, M.; Wu, W.; Woo, E. P.; Grell, M.; Bradley, D. D. C. *Appl. Phys. Lett.* **2000**, *77*, 406.

(13) Morana, M.; Bret, G.; Brabec, C. *Appl. Phys. Lett.* **2005**, *87*, 153511.

(14) (a) Lu, G.; Usta, H.; Risko, C.; Wang, L.; Facchetti, A.; Ratner, M. A.; Marks, T. J. *J. Am. Chem. Soc.* **2008**, *130*, 7670. (b) Werzer, O.; Matoy, K.; Smilgies, D. −M.; Rothmann, M. M.; Strohriegl, P.; Resel, R. *J. Appl. Polym. Sci.* **2008**, *107*, 1817.

(15) (a) Grozema, F. C.; Siebbeles, L. D. A.; Warman, J. M.; Seki, S.; Tagawa, S.; Scherf, U. *Adv. Mater.* **2002**, *14*, 228. (b) Grozema, F. C.; Warman, J. M. *Radiat. Phys. Chem.* **2005**, *74*, 234.

(16) Saeki, A.; Seki, S.; Takenobu, T.; Iwasa, Y.; Tagawa, S. *Adv. Mater.* **2008**, *20*, 920.

(17) (a) Yamamoto, Y.; Zhang, G.; Jin, W.; Fukushima, T.; Ishii, N.; Saeki, A.; Seki, S.; Tagawa, S.; Minari, T.; Tsukagoshi, K.; Aida, T. *Proc. Natl. Acad. Sci.* **2009**, *106*, 21051. (b) Kocherzhenko, A. A.; Patwardhan, S.; Grozema, F. C.; Anderson, H. L.; Siebbeles, L. D. A. *J. Am. Chem. Soc.* **2009**, *131*, 5522. (c) Pingel, P.; Zen, A.; Abellón, R. D.; Grozema, F. C.; Siebbeles, L. D. A.; Neher, D. *Adv. Funct. Mater.* **2010**, *20*, 2286. (d) Saeki, A.; Seki, S.; Shimizu, Y.; Yamao, T.; Hotta, S. *J. Chem. Phys.* **2010**, *132*, 134509.

(18) (a) Ie, Y.; Nitani, M.; Uemura, T.; Tominari, Y.; Takeya, J.; Honsho, Y.; Saeki, A.; Seki, S.; Aso, Y. *J. Phys. Chem. C* **2009**, *113*, 17189. (b) Zhang, W.; Ochi, K.; Fujiki, M.; Naito, M.; Ishikawa, M.; Kaneto, K.-i.; Takashima, W.; Saeki, A.; Seki, S. *Adv. Funct. Mater.* **2010**, *20*, 3941. (c) Terao, J.; Tanaka, Y.; Tsuda, S.; Kambe, N.; Taniguchi, M.; Kawai, T.; Saeki, A.; Seki, S. *J. Am. Chem. Soc.* **2009**, *131*, 18046.

(19) (a) Saeki, A.; Seki, S.; Koizumi, Y.; Tagawa, S. *J. Photochem. Photobiol. A* **2007**, *186*, 158. (b) Saeki, A.; Seki, S.; Sunagawa, T.; Ushida, K.; Tagawa, S. *Phil. Mag.* **2006**, *86*, 1261.

(20) (a) Barbarellu, G.; Casarini, D.; Zambianchi, M.; Favaretto, L.; Rossini, S. *Adv. Mater.* **1996**, *8*, 69. (b) Azumi, R.; Goto, M.; Honda, K.; Matsumoto, M. *Bull. Chem. Soc. Jpn.* **2003**, *76*, 1561. (c) Melucci, M.; Gazzano, M.; Barbarella, G.; Cavallini, M.; Biscarini, F.; Maccagnani, P.; Ostoja, P. *J. Am. Chem. Soc.* **2003**, *125*, 10266.

(21) Clot, O.; Selmarten, D.; McNevin, M. J. *J. Mater. Chem.* **2005**, *15*, 4934.

(22) Nagamatsu, S.; Kaneto, K.; Azumi, R.; Matsumoto, M.; Yoshida, Y.; Yase, K. *J. Phys. Chem. B* **2005**, *109*, 9374.

(23) Meng, H.; Zheng, J.; Lovinger, A. J.; Wang, B. C.; Van Patten, P. G.; Bao, Z. *Chem. Mater.* **2003**, *15*, 1778.

(24) He, M.; Li, J.; Sorensen, M. L.; Zhang, F.; Hancock, R. R.; Fong, H. H.; Pozdin, V. A.; Smilgies, D. −M.; Malliaras, G. G. *J. Am. Chem. Soc.* **2009**, *131*, 11930.

(25) (a) Leclerc, M.; Faid, K. *Adv. Mater.* **1997**, *9*, 1087. (b) Bolognesi, A.; Giacometti Schieroni, A.; Botta, C.; Marinelli, M.; Mendichi, R.; Rolandi, R.; Relini, A.; Inganäs, O.; Theandher, M. *Synth. Met.* **2003**, *139*, 303.